Astronomy & Astrophysics manuscript no. output
November 22, 2024
©ESO 2024

The *R*-Process Alliance: Hunting for Gold and other elements with lines in the near-UV spectrum

Terese T. Hansen[1], Ian U. Roederer[2,3], Shivani Shah[4], Rana Ezzeddine[4,3], Timothy C. Beers[5,3], Anna Frebel[6,3], Erika M. Holmbeck[7,3], Vinicius M. Placco[8], Charli M. Sakari[9], Alexander Ji[10], and Jennifer L. Marshall[11]

[1] Department of Astronomy, Stockholm University, AlbaNova University Center, SE-106 91 Stockholm, Sweden e-mail: thidemannhansen@gmail.com
[2] Department of Physics, North Carolina State University, Raleigh, NC 27695, USA
[3] Joint Institute for Nuclear Astrophysics – Center for the Evolution of the Elements (JINA-CEE), USA
[4] Department of Astronomy, University of Florida, Bryant Space Science Center, Gainesville, FL 32611, USA
[5] Department of Physics and Astronomy, University of Notre Dame, Notre Dame, IN 46556, USA
[6] Department of Physics and Kavli Institute for Astrophysics and Space Research, Massachusetts Institute of Technology, Cambridge, MA 02139, USA
[7] Lawrence Livermore National Laboratory, 7000 East Avenue, Livermore, CA 94550, USA
[8] NSF's NOIRLab, Tucson, AZ 85719, USA
[9] Department of Physics and Astronomy, San Francisco State University, San Francisco, CA 94132, USA
[10] Department of Astronomy & Astrophysics, University of Chicago, 5640 S Ellis Avenue, Chicago, IL 60637, USA
[11] Mitchell Institute for Fundamental Physics and Astronomy and Department of Physics and Astronomy, Texas A&M University, College Station, TX 77843-4242, USA

November 22, 2024

ABSTRACT

Context. Over the past years, the *R*-Process Alliance (RPA) have successfully carried out a search for stars highly enhanced in elements produced in the rapid neutron-capture (*r*-)process. In particular, the RPA has identified a number of *r*-process stars suitable for observations with the Hubble Space Telescope (HST), facilitating abundance derivation of elements such as Gold and Cadmium.
Aims. This paper presents the detailed abundances derived for the highly *r*-process enhanced star 2MASS J05383296-5904280, the third RPA star observed with the HST, significantly increasing the sample of *r*-process stars with near-UV observations.
Methods. 1D LTE elemental abundances are derived via equivalent width and spectral synthesis using high-resolution high signal-to-noise near-UV HST/STIS and optical Magellan/MIKE spectra.
Results. Abundances are determined for 43 elements, including 26 neutron-capture elements. In particular, abundances of Nb, Mo, Cd, Lu, Os, Pt, and Au are derived from the HST spectrum. Increasing the number of Cd abundances derived in *r*-process stars from seven to ten and Au abundances from four to seven. For both these elements, a large star-to-star scatter is detected, highlighting the need for more detections and further investigation of these elements.

Key words. Stars: abundances – Galaxy: halo

1. Introduction

The origin and chemical evolution of elements such as gold and silver have long been investigated in nuclear astrophysics. These elements, along with half of the other isotopes heavier than iron, are produced via the rapid-neutron capture process or *r*-process. This process was theoretically predicted almost 70 years ago (Burbidge et al. 1957; Cameron 1957), but the astrophysical site(s) of this process is still heavily debated. A strong candidate for an astrophysical site is neutron star mergers (NSMs) as suggested by Lattimer & Schramm (1974). This was confirmed in 2017 when The Laser Interferometer Gravitational-Wave (LIGO) observatory detected a signal from an NSM (Abbott et al. 2017). Extensive photometric and spectroscopic observations of the corresponding kilonova sss17a revealed a signal consistent with the decay of heavy-element isotopes produced in the merger(Drout et al. 2017). Potentially, 3–13 Earth masses of gold were produced in this event (Côté et al. 2018). However, there are large uncertainties in the assumed abundance composition resulting from this one event Côté et al. (2018). Furthermore, galactic chemical evolution models and the contents of neutron-capture elements in the oldest stars in the Milky Way (MW) halo and satellites suggest that NSMs may not be the only site of *r*-process element production (Côté et al. 2017). Since the discovery of SSS17a, a renewed interest in the *r*-process has resulted in a theoretical effort to identify additional heavy element production sites. Currently, in addition to NSMs and neutron star - black hole mergers (Lattimer & Schramm 1974; Wehmeyer et al. 2019), various types of SNe such as collapsars (Siegel et al. 2019), magneto-rotationally driven SNe (Fujimoto et al. 2008), and common envelope jet SNe(Grichener & Soker 2019) have been suggested.

Since direct observations of *r*-process element-production sites such as NSMs and exotic SNe are still very sparse, and new observations will be hard to obtain as these events are rare and often also faint, we need to look for clues concerning the details of the *r*-process in other places. An ideal place is the abundances of the oldest and most metal-poor stars in the Milky Way (MW). The chemical composition of these stars, mapped through detailed abundance analysis, is a direct fingerprint of the elements produced in the stellar generation before them. In 2016, The *R*-Process Alliance (RPA) initiated a successful search for *r*-process enhanced stars to investigate the *r*-process. In the first five data release papers (Hansen et al. 2018; Sakari et al. 2018; Holmbeck et al. 2020; Ezzeddine et al. 2020; Bandyopadhyay et al. 2024) the RPA has discovered over 70 highly *r*-process enhanced *r*-II stars ([Eu/Fe] $>$ 0.7; Holmbeck et al. (2020)) and several hundred mildly enhanced *r*-I stars (0.3 $<$ [Eu/Fe] $<$ 0.7; Holmbeck et al. (2020)). For several of these stars, the RPA has been able to derive extremely detailed *r*-process element abundance patterns including more than 20 neutron-capture elements e.g., HD 222529 (Roederer et al. 2018b, 2022b), 2MASS J09544277+5246414 (Holmbeck et al. 2018), RAVE J183013.5-455510 (Placco et al. 2020), and 2MASS J1521399-3538094 (Cain et al. 2020) revealing new details on the *r*-process.

However, abundances for a number of neutron-capture elements, such as cadmium (Cd) and gold (Au), can not be obtained from ground-based observation as these elements only display absorption features in the near-ultraviolet (near-UV) region of the electromagnetic spectrum. Hence, part of the RPA survey effort has also been focused on identifying stars for which near-UV spectra could be obtained with the Hubble Space Telescope (HST) to investigate the behaviour of these additional neutron-capture elements in *r*-process stars. Here, we present the detailed abundance analysis of the third RPA star observed in near-UV with the HST, namely 2MASS J05383296-5904280, J0538 hereafter. The other two RPA stars with near-UV HST spectra are J0051, for which (Shah et al. 2024) derived the highest Au abundance seen in an *r*-process enhanced star to date, and HD 222529 for which Roederer et al. (2022b) derived the most complete abundance pattern of any object outside the Solar system, including 42 neutron-capture elements. Abundances of Au have been derived in all three stars, almost doubling the number of Au abundances available for *r*-process stars in the literature and allowing us for the first time to investigate the behavior of this element.

This paper is organized as follows: Section 2 describes the optical and near-UV observations J0538 and the analysis is described in Section 3, Section 4 presents our results, which are discussed in Section 5, and Section 6 provides a summary.

2. Observations

2.1. Optical

The star was first observed as part of the RPA snapshot survey (Hansen et al. 2018) on November 24, 2017, with the echelle spectrograph on the du Pont telescope (Bowen & Vaughan 1973). The analysis was published in the fourth RPA data release (Holmbeck et al. 2020), which determined an Eu abundance of [Eu/Fe] = 1.28, and a [Ba/Eu] = −0.52 classifying it as an *r*-II star. A portrait spectrum was therefore obtained with the MIKE spectrograph (Bernstein et al. 2003) on November 15, 2018. Two 1200 sec exposures were obtained using the 0.5" x 5.0" slit and 2x1 binning, yielding a resolving power of $R \sim 55,000$ in the blue and $R \sim 45,000$ in the red and with a spectral coverage of 3330-5060 Å and 4850-9400 Å in the blue and red channels respectively. The data was reduced using the CarPy software (Kelson 2003) with the final spectra having a signal-to-noise ratio (SNR) of 335 at 4500 Å

2.2. Near-UV

A near-UV spectrum of the star was obtained with HST/STIS (Kimble et al. 1998; Woodgate et al. 1998) on 2020 April 16 and 21 (Hansen et al. 2019, Proposal ID: 15951). The observations were carried out using the E230M echelle grating centered at λ2707 Å providing a wavelength coverage of ~2275–3119 Å and with the 0.2" × 0.2" slit, yielding a resolving power of $R \sim$ 30,000. The star was observed over five orbits, with three orbits in the first visit and two in the second. The total exposure time over the five orbits was ~3.63 hours. The spectra were processed automatically by the CALSTIS software package and downloaded from the Mikulski Archive for Space Telescopes. Each of the five spectra was cross-correlated against a spectrum of the star HD84937 (V_{helio}= -15.05 Gaia Collaboration (2018)) obtained with the same setup and shifted to rest velocity. The shifted spectra were then normalized and co-added, resulting in an SNR of 44 at 2707 Å in the final spectrum.

2.3. Binarity

The star exhibits radial-velocity variations, suggesting it is a binary. We, therefore, obtained additional spectra of the star with the MIKE spectrograph for radial velocity measurements using the 0.7"x5" slit and 2x2 bin. Each velocity is obtained via cross-correlation with a spectrum of the radial velocity standard star HD122563 (V_{helio}= -26.13 Gaia Collaboration (2018)) obtained with the same setting as the target star. The reported velocity is the mean of the orders used and the standard deviation. Final velocities are listed in Table 2. We also compute an orbit...

3. Stellar parameter determination and abundance analysis

The stellar parameters were determined following the RPA procedure (see e.g. Roederer et al. (2022b); Shah et al. (2024)). Effective temperatures $T_{\rm eff}$ are derived from the Gaia G, BP, and RP, and 2MASS K magnitudes using the color-temperature relations form Mucciarelli et al. (2021). The *Gaia* magnitudes were de-reddened following (Babusiaux et al. 2023) and using the $E(B-V)$ value listed in Table 1 obtained from the Schlafly & Finkbeiner (2011) dust maps. To de-redden the K magnitude, we use the extinction coefficient from McCall (2004). Following the $T_{\rm eff}$ determination, we determine log g from the fundamental relation:

$$\log g = 4\log T_{\rm eff} + \log(M/\,{\rm M}_\odot) - 10.61 + 0.4\cdot(BC_V + m_V - 5\log(d) + 5 - 3.1\cdot E(B-V) - M_{\rm bol,\odot}). \quad (1)$$

Here, M is the mass of the star, assumed to be 0.8 ± 0.08 $M_\odot$. BC_V is the bolometric correction in the V band (Casagrande & VandenBerg 2014), m_V is the apparent Vmagnitude, d is the distance in PC from Bailer-Jones et al. (2021), and $M_{\rm bol,\odot}$ is the solar bolometric magnitude, 4.75. The constant 10.61 is calculated from the solar constants $\log(T_{\rm eff})_\odot$ = 3.7617 and log $g_\odot$ = 4.438. Finally, the model atmosphere metallicity [M/H] and microturbulence ξ are determined from equivalent width (EW) measurements of Fe I and Fe II lines, using the [FeII/H] abundance as model atmosphere metallicity. The final stellar parameters are listed in Table 1. Systematic uncertainties on $T_{\rm eff}$ and log g and corresponding effects on [Fe/H] and ξ are determined from (Ian, Vini) resulting in $\delta T_{\rm eff}/\delta \log g/\delta\,[{\rm Fe/H}]/\delta\xi$ = 47/0.07/0.04/0.1, statistical uncertainties are based on the scatter in individual Fe I and Fe II line abundances used, resulting

Table 1. Properties of 2MASS J05383296-5904280

Quantity	Symbol	Value	Unit	Ref
R.A.	α(J2000)	05:38:32.96	hh:mm:ss.ss	Simbad
Decl.	δ(J2000)	-59:04:28.11	hh:mm:ss.ss	Simbad
Galactic longitude	l	267.7	degrees	Simbad
Galactic latitude	b	-32.3	degrees	Simbad
Parallax	ϖ	0.8804±0.0109	mas	Gaia Collaboration et al. (2023)
Inverse parallax distance	$1/\varpi$	±	pc	This work
Distance	d	1128.11	pc	Bailer-Jones et al. (2021)
Mass	Mass	0.80±0.08	$M_{\odot}$	Assumed
V magnitude	V	9.89	mag	Munari et al. (2014)
G magnitude	G	9.60	mag	Gaia Collaboration et al. (2023)
BP magnitude	BP	9.91	mag	Gaia Collaboration et al. (2023)
RP magnitude	RP	9.10	mag	Gaia Collaboration et al. (2023)
A_0 magnitude	A_0		mag	Gaia Collaboration et al. (2023)
K magnitude	K	8.12	mag	Cutri et al. (2003)
Color excess	$E(B-V)$	0.056	mag	Schlafly & Finkbeiner (2011)
Bolometric correction	BC_V		mag	Based on Casagrande & VandenBerg (2014)
Effective Temperature	$T_{\rm eff}$	5819±57	K	This work
Log of surface gravity	$\log g$	2.09±0.08	(cgs)	This work
Microturbulent velocity	ξ	2.60±0.05	kms^{-1}	This work
Model metallicity	[M/H]	-2.55±0.07	dex	This work

Notes.

Table 2. Heliocentric radial velocities measured for J0538.

MJD	V$_{helio}$ kms^{-1}	σ kms^{-1}
58081.28257*	189.09	0.37
58437.51464*	188.59	0.34
59641.51270	197.33	0.64
230127		
240830		

Notes. * snapshot and portrait spectra.

in $\delta T_{\rm eff}/\delta \log g/\delta$ [Fe/H]$/\delta\xi$ = 36/0.03/0.06/0.17, total parameter uncertainties added in quadrature are listed in Table 1

Abundances for J0538 have been derived via EW analysis and spectral synthesis using the analysis code `SMHR`[1] to run the 1D radiative transfer code `MOOG`[2](Sneden 1973; Sobeck et al. 2011), assuming local thermodynamical equilibrium (LTE). α-enhanced ([α/Fe] = +0.4) `ATLAS9` model atmospheres (Castelli & Kurucz 2003) and line lists generated from `linemake`[3] (Placco et al. 2021) with updates following Roederer et al. (2018b, 2022b) were used as input, and Solar abundances were taken from Asplund et al. (2009). The synthesis also includes isotopic and hyperfine structure broadening, where applicable, employing the *r*-process isotope ratios from Sneden et al. (2008). Table A.1 in the appendix lists the atomic data for the lines used in the analysis, along with the measured EW and abundance of each line.

4. Results

We derive abundances for 43 elements and 51 species. Table 4 lists the final abundances and associated uncertainties. For 30 species, we identify and analyze lines in the near-UV spectrum abundances derived for these elements are listed explicitly in Table 3. The abundance uncertainties are determined by propagating through the stellar parameter uncertainties following the procedure outlined in Ji et al. (2020). This method performs a line-by-line analysis and includes both statistical and systematic uncertainties. We add 0.2 dex uncertainty to all abundances derived from two or fewer lines and 0.1 dex to all abundances to account for continuum placement, atomic data uncertainties, and other systematic uncertainties. A summary of the uncertainties is given in Table 5.

4.1. Elements with Z<31

We derive abundances for 17 elements in this group from Oxygen to Zink. In addition, we derive 3σ upper limits on C from the CH-G band ([C/Fe] < -0.97), on N from the NH 3360 Å band ([N/Fe] < 0.77), and Cu from the 5105 Å line ([Cu/Fe] < -0.69). In Figure 1, we plot the abundances derived for light elements in J0538 (pink star) compared to those of the other two RPA stars with HST spectra (HD222925: green cross, J0051: blue square), and abundances from Milky Way halo stars (Roederer et al. 2014a). Generally, the abundances of the light elements in the three RPA HST stars agree quite well with the general Milky Halo population. We do note that J0538 has high O ([O/Fe] = 1.03), Na ([Na/Fe] = 0.90), and K ([K/Fe] = 0.84) abundances. High O and Na abundances are sometimes seen in connection with carbon enhancement (Yoon et al. 2016, and references therein). However, the low upper limit we derive for C rules out a CEMP classification of the star (Carbon Enhanced Metal-Poor; [C/Fe] > 0.7 Beers & Christlieb (2005); Aoki et al. (2007)). For a number of elements, we derive abundance from both neutral and ionized lines, in particular, facilitated by the HST spectrum for the elements Al, Si, Co, and Ni (see Figure 2). The abundances derived from the different ionization states deviate for some of these elements, likely due to departures from the LTE assumption employed in this work. For Al, we find [AlI/Fe] = -0.57 and [AlII/Fe] = $+0.02$ using the 3944 and

[1] https://github.com/andycasey/smhr
[2] https://github.com/alexji/moog17scat
[3] https://github.com/vmplacco/linemake

Table 3. UV Abundance Summary for J0538.

El.	N	$\log \epsilon$ (X)	[X/H]	$\sigma_{[X/H]}$ [dex]	[X/Fe]	$\sigma_{[X/Fe]}$ [dex]
Mg I	4	+5.37	−2.23	0.05	+0.37	0.05
Al I	3	+3.24	−3.21	0.22	−0.62	0.22
Al II	1	+3.87	−2.58	0.23	+0.02	0.23
Si I	3	+5.21	−2.30	0.11	+0.30	0.11
Si II	2	+5.67	−1.84	0.19	+0.75	0.20
P I	1	+2.69	−2.72	0.26	−0.13	0.26
Ca I	1	+3.81	−2.53	0.09	+0.06	0.09
Sc II	1	+1.20	−1.95	0.17	+0.65	0.18
Ti I	3	+2.75	−2.20	0.08	+0.39	0.08
Ti II	13	+2.86	−2.09	0.04	+0.50	0.05
V II	14	+1.61	−2.32	0.05	+0.27	0.06
Cr I	4	+2.83	−2.81	0.07	−0.21	0.07
Cr II	10	+3.29	−2.35	0.05	+0.24	0.06
Fe I	19	+4.91	−2.59	0.02	...	...
Fe II	4	+4.98	−2.52	0.04	+0.08	...
Co II	6	+2.48	−2.51	0.11	+0.08	0.11
Ni I	16	+3.64	−2.58	0.05	+0.01	0.05
Ni II	4	+3.90	−2.32	0.29	+0.27	0.29
Y II	1	−0.14	−2.35	0.15	+0.24	0.16
Zr II	10	+0.58	−2.00	0.05	+0.59	0.06
Nb II	3	−0.34	−1.80	0.16	+0.79	0.16
Mo II	4	+0.14	−1.74	0.08	+0.86	0.08
Cd I	1	−0.36	−2.07	0.26	+0.52	0.26
Gd II	5	−0.33	−1.40	0.07	+1.19	0.08
Er II	1	−0.41	−1.33	0.22	+1.26	0.23
Lu II	1	−1.16	−1.26	0.25	+1.33	0.26
Hf II	1	−1.17	−2.02	0.83	+0.57	0.83
Os II	1	−0.10	−1.50	0.27	+1.09	0.27
Pt I	4	+0.22	−1.40	0.17	+1.20	0.17
Au I	2	−0.78	−1.70	0.21	+0.89	0.21

3961Ålines. The difference between our Al abundances corresponds to the non-LTE correction for Al I of 0.53 dex found by Lind et al. (2022) for the benchmark star with similar parameters, HD140283 ($T_{\rm eff}$ =5792, log g =3.65, [Fe/H]= -2.38). We find a 0.45 dex difference between our Si I and Si II abundances, but the MPIA-based non-LTE correction tool[4] find no correction for the 3905ÅSiI line for this star based on the grid from (Bergemann et al. 2013)[5]. We find good agreement between our Ti I and Ti II, and Co I and Co II abundances. The recent work by Mallinson et al. (2022), however, suggests a non-LTE correction of +0.22 dex should be applied to the Ti I, and +0.03 dex to the Ti II abundances of the benchmark star HD140283 (same as the one used above for Al). Also, for Co, non-LTE corrections as high as +0.6-0.8 dex were found for Co I lines in metal-poor stars by Bergemann et al. (2010). In our analysis, Cr, Mn, and Ni display larger offsets between abundances from neutral and ionized species. Using the MPIA-based non-LTE correction tool, we find non-LTE corrections of +0.65 - +0.88 for the Cr I lines used in this analysis, based on the grid from Bergemann & Cescutti (2010), which are significantly larger than the 0.31 dex abundance offset we find between Cr I and Cr II. Using the same tool, we find corrections of +0.4 - +0.6 dex for the Mn I lines used, based on the grid from Bergemann & Gehren (2008), closer to our abundance offset of 0.24 dex. Eitner et al. (2023) recently computed the non-LTE effects for Ni and determined a correction of +0.15 dex for Ni I abundances for stars in our parameter regime, bringing our Ni I abundances closer to the Ni II value.

[4] https://nlte.mpia.de/gui-siuAC_secE.php

[5] The other Si I lines used are in the UV and no non-LTE analysis exists for these to our knowledge.

4.2. Neutron-Capture Elements

We derive abundances for 26 neutron-capture elements from Sr to Th. This includes abundances of Nb, Mo, Cd, Lu, Os, Pt, and Au, exclusively derived from the near-UV HST spectrum. Figure 2 shows the synthesis of selected lines of these elements. J0538 has a Ba to Eu ratio of $[Ba/Eu] = -0.56$, and in Figure 3, we plot the $\log_\epsilon$(X) abundances of the neutron-capture elements detected in J0538 as a function of atomic number compared to the solar r- and s- process abundances patterns clearly showing the agreement with the r-process pattern, confirming the r-process origin of the neutron-capture elements in the atmosphere of this star.

5. Discussion

J0538 is the third r-II star for which the RPA has obtained near-UV spectra with the HST. In all three stars, we have derived abundances of Cd and Au, increasing the sample of Cd abundances from seven to ten and Au abundances from four to seven. In the following, we will discuss the abundance signatures of Cd and Au in r-process stars in relation to two recent RPA discoveries, namely the universal light r-process element pattern (Roederer et al. 2022a) and the fission fragment deposition signature (Roederer et al. 2023). For this discussion, we make two plots, Figure 4 and 5, showing the neutron-capture element abundances derived for our three RPA HST stars: J0538 (pink), HD222925 (green) and J0051 (blue), along with literature stars with Cd (Figure 4) and Au (Figure 5) compared to the baseline pattern from Roederer et al. (2023). Elements from Sr to Cd are scaled to Zr, while the heavy neutron-capture elements from Ba to Au, are scaled to Ba, and circle sizes are correlated with [Eu/Fe] ratios, such that the largest circles represent the stars with highest [Eu/Fe] ratios and vice versa.

5.0.1. Light r-process elements, including Cd

Literature stars included in Figure 4 are HD 140283 ($\log_\epsilon$(Cd) = -1.46; Peterson et al. (2020)), HD 128279 ($\log_\epsilon$(Cd) = -1.38; Roederer et al. (2012, 2014b, 2022a)), HD 19445 ($\log_\epsilon$(Cd) = -0.36; Peterson et al. (2020)), HD 84937 ($\log_\epsilon$(Cd) = -0.36;Peterson et al. (2020)), HD 160617 ($\log_\epsilon$(Cd) = -0.03; Roederer & Lawler (2012); Peterson et al. (2020)), HD 108317 ($\log_\epsilon$(Cd) = -1.15; Roederer et al. (2012, 2014b, 2022a)), and BD+17°3248 ($\log_\epsilon$(Cd) = 0.99; Cowan et al. (2002); Sneden et al. (2009); Den Hartog et al. (2005); Roederer et al. (2022a)). From Figure 4 we see that our three RPA HST stars and the literature sample all agree with the recently discovered universality among light r-process elements extending up to Mo (Roederer et al. 2022a). A slightly larger scatter is seen for Sr, driven by the high Sr abundances of J0538. This high Sr abundance could be connected to the elevated O and Na abundances found for this star as mentioned in Section 4 and may result from extensive mixing and processing in a metal-free, fast-rotating, so-called spinstar progenitor Maeder & Meynet (2015).

For the elements from Ru to Ag, we see the fission fragment deposition signature discovered by Roederer et al. (2023) where the abundances of these elements are correlated with the Eu abundance of the stars. Moving on to Cd, a much larger spread

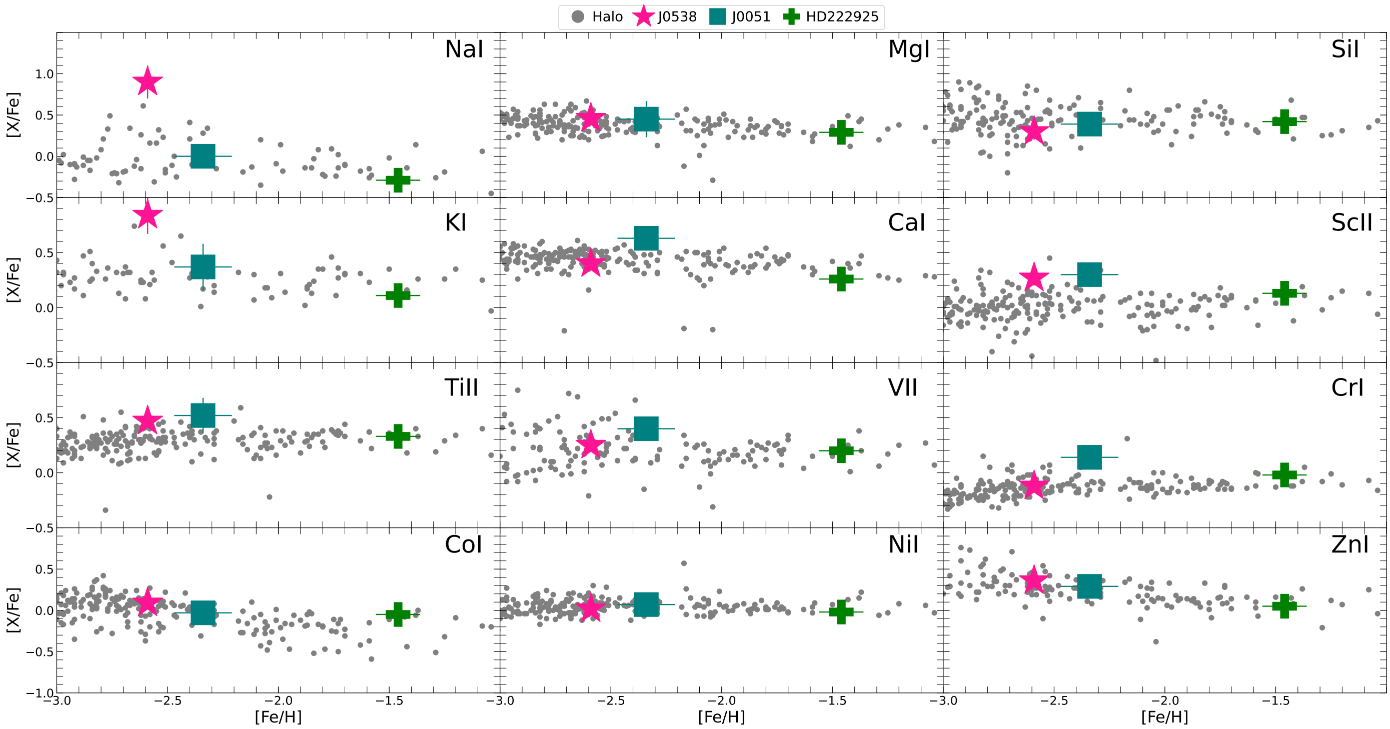

Fig. 1. [X/Fe] derived abundances for the three RPA HST stars: J0538 (pink star), HD222925 (green cross,Roederer et al. (2022b)), and J0051: (blue square,Shah et al. (2024)) compared to stellar abundances from the MW halo (grey dots; Roederer et al. 2014a).

between the stars and no clear correlation with Eu abundances is seen in the abundances of this element. This is somewhat driven by the very high Cd abundances derived for J0051 by Shah et al. (2024). Shah et al. (2024) investigated this spread and found correlations of the derived Cd abundances with the stellar parameters $T_{\rm eff}$ and log g of the stars, suggesting that non-LTE effects might affect the Cd abundances. The Cd abundance we derive for J0538 [Cd/Fe] = 0.52 along with the $T_{\rm eff}$ and log g has J0538 following the correlations found in Shah et al. (2024) thus supporting the suspected non-LTE effects.

5.0.2. Heavy *r*-process elements, including Au

The four *r*-process stars present in the literature with Au abundances, reported before the RPA, and included in Figure 5 are HD 108317 ($\log_\epsilon$(Au) = -1.64; Roederer et al. (2012, 2014b, 2022a)), BD+17°3248 ($\log_\epsilon$(Au) = -0.60; (Roederer et al. 2022a)), CS 22892–052 ($\log_\epsilon$(Au) = -0.90; (Sneden et al. 2003)), and CS 31082–001 ($\log_\epsilon$(Au) = -1.00; (Siqueira Mello et al. 2013)). We note that the only two literature stars, namely HD 108317 and BD+17°3248 appear both in Figure 4 and 5; the RPA has thus more than doubled the number of *r*-process stars for which abundances of both Cd and Au has been derived. Similar to Cd, we see a somewhat larger scatter for Au in Figure 5 compared to the other heavy *r*-process and no clear correlation between an increased Au abundance and an increased Eu abundance. It should be noted that Roederer et al. (2023) did not include Lu, Ta, W, Re, and Ir in their sample; hence, the baseline pattern (grey line) in Figure 5 is not representative for these two elements.

The scatter in Au abundances between the stars is also apparent when performing the standard exercise of comparing the neutron-capture element abundances of the *r*-process star to the scaled Solar System *r*-process pattern, as done in Figure 3 for J0538. Here the seven stars with Au detections fall into two categories, the Au abundances in BD+17°3248, J0051, and HD222529 follow the scaled Solar System *r*-process pattern (Cowan et al. 2002; Shah et al. 2024; Roederer et al. 2022b), while the Au abundances in HD 108317, CS 22892-052, CS 31081-001, and J0538 all fall below the scaled pattern (Roederer et al. 2012; Siqueira Mello et al. 2013; Sneden et al. 2003).

Several studies have found that the shape and position of the third *r*-process peak is highly influenced by the choice of fission, fission fragment distribution, and adopted β-decay rates, which can lead to late-time neutron captures (Surman & Engel 2001; Eichler et al. 2015; Lund et al. 2023). Roederer et al. (2023) found a correlation between the abundance of Eu and the third-peak elements Os and Pt in their sample of *r*-process stars, suggesting that the ratios of these elements to Eu are possibly affected by fission fragment deposition. Au was not included in this study due to the small number of abundances derived for this element. However, the large spread in Au abundances seen in Figure 5 compared to Os and Pt highlights Au as an element needing further investigation.

The Au abundances in all of these stars use the Au I line at 2675 Å and all but one use atomic data from Hannaford et al. (1981) $\log gf = -0.45$, the study of HD 108317 uses atomic data from Fivet et al. (2006) with almost identical $\log gf = -0.47$. However, while this study and that of J0051, HD 222925, and BD+17°3248 include HFS (Demidov et al. 2021), there is no mention of this in the studies of HD 108317, CS 31081-001, and CS 22892-052. We tested the effect of excluding the HFS components from our line list and found a change in the Au abundance of J0538 of −0.05 dex. Hence, this is not likely the source of the spread seen in the Au abundances between these stars. It is possible, however, that these abundances are affected by non-LTE effects, similar to the Cd abundances. For completeness, we

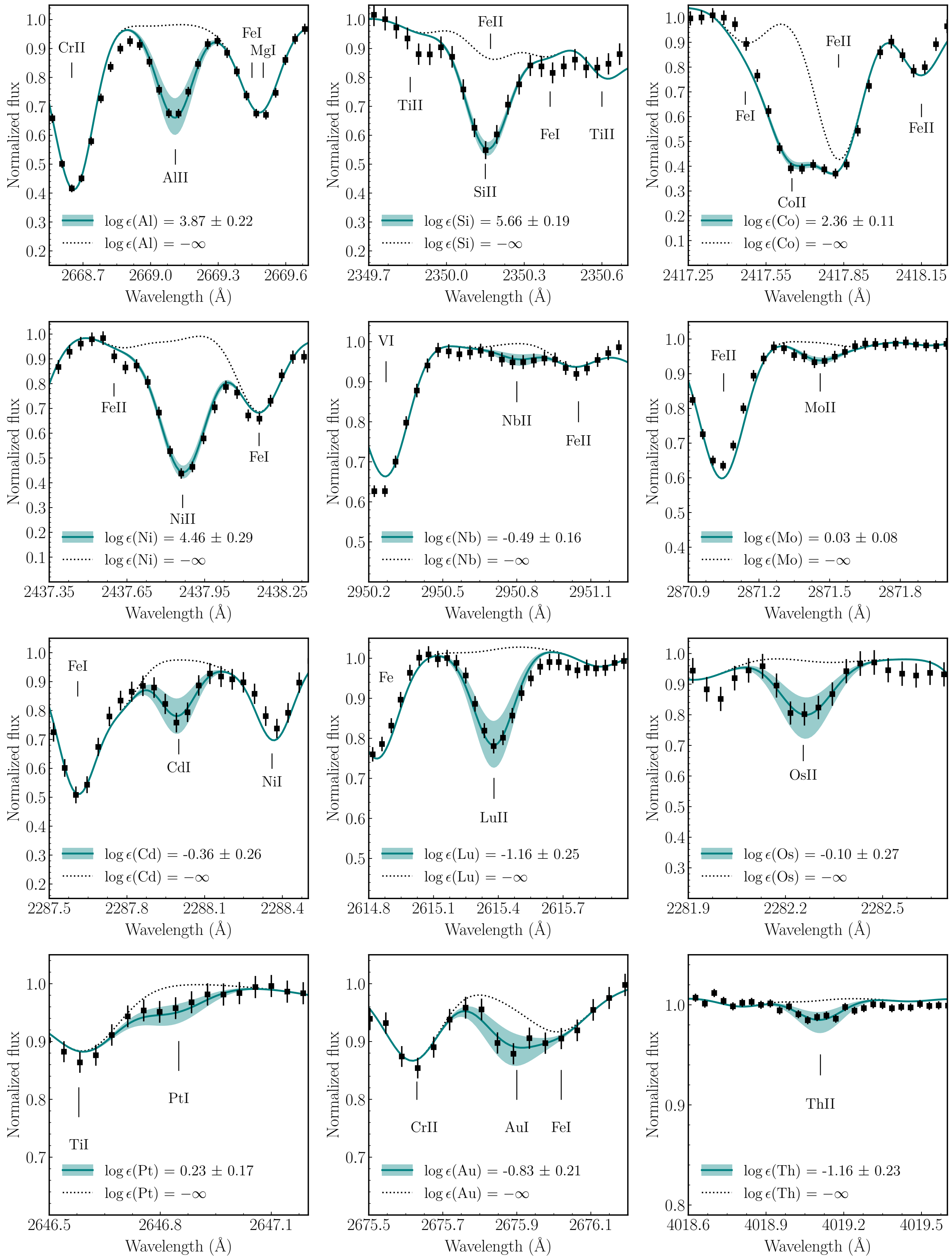

Fig. 2. Comparison of synthesis and observed spectra (black line) for selected absorption features in the near-UV spectrum and Th. The blue line is the best-fit synthesis, the blue band shows the uncertainty, and the dotted line is a synthesis without the given element.

note that in J0538 and J0051, the Au I line at 2427 Å was also used to derive the final Au abundance.

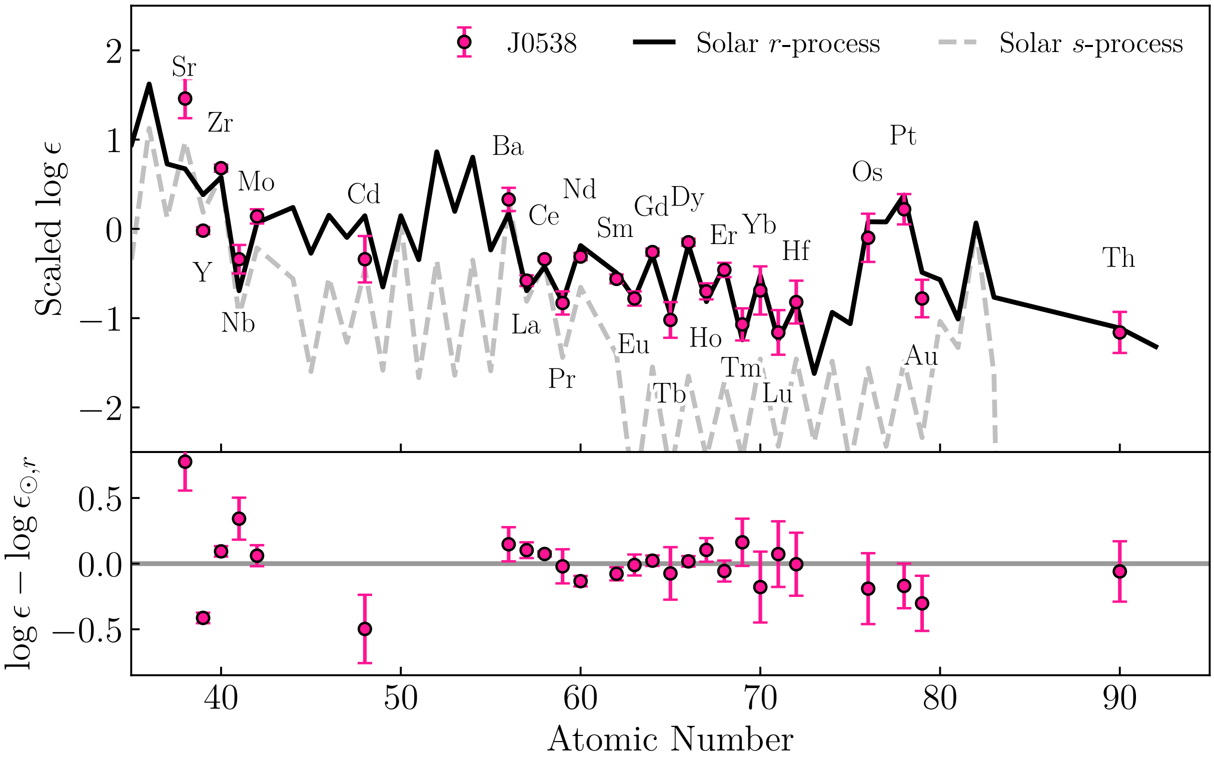

Fig. 3. Absolute abundances for neutron-capture elements derived for J0538 compared to scaled Solar system $r-$ (solid) and s-process (dashed) abundances taken from (Sneden et al. 2008). The stellar abundances most closely match the Solar system r-process abundance pattern.

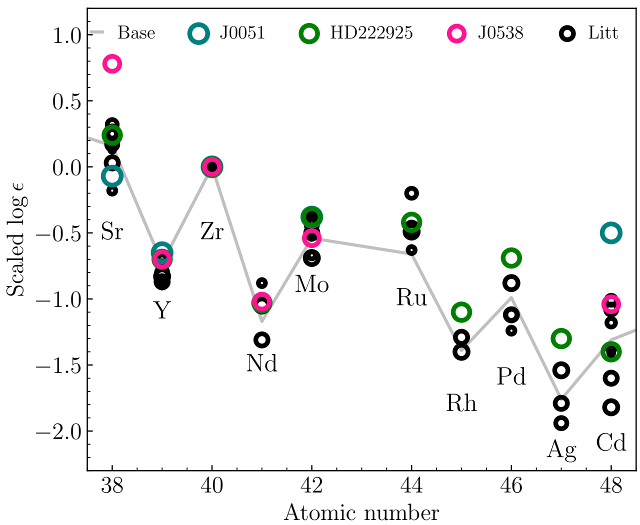

Fig. 4. Absolute abundances of light r-process elements for the three RPA HST stars (pink, green, and blue) and literature stars (black) with Cd detections compared to the baseline pattern from Roederer et al. (2023). Point size is correlated with the Eu abundance of the star. Elements from Sr to Mo follow the universal light element pattern, while signatures of fission fragment deposition are seen for Ru to Ag. Cd displays a larger scatter and no clear correlation with Eu abundances

5.1. Dynamical signature of J0538

The dynamical properties of J0538 were explored by Gudin et al. (2021) and Shank et al. (2023) using *Gaia* data. Gudin et al. (2021) found J0538 to belong to their identified chemo-dynamical tied group #6 (CDTG-6) along with the two r-I stars HD 149414 (Fulbright 2000) and 2MASS J01373857-2618131 (Holmbeck et al. 2020). Previous kinematic analyses have found a large number of r-process stars, including stars from the literature sample used in Figure 4 and 5 to belong to groups characterized by the stars having similar orbital parameters and metallicities (Roederer et al. 2018a). Thus, these r-process stars likely formed in a low-mass MW satellite, which was later accreted by the MW. Further identification and exploration of these systems are key to investigating the r-process signature in metal-poor stars.

6. Summary

This paper presents the detailed abundances derived from optical and near-UV spectra of the r-process-enhanced star J0538. This is the third star discovered by the RPA for which near-UV spectra with the HST have been obtained, significantly increasing the sample of r-process stars with abundances derived from near-UV spectra. We derive abundances for 43 elements, including 26 neutron-capture elements and 25 from the HST spectrum. In particular, we derive abundances for the neutron-capture elements Cd and Au. Prior to the RPA analysis, only two r-process stars existed in the literature, with abundances for both elements reported. We investigate the behaviour of these two elements in r-process stars in relation to the recently discovered fission fragment deposition signature potentially affecting the neutron-capture element abundances in r-process stars up to the third peak elements Os and Pt. For both elements, a larger star-to-star

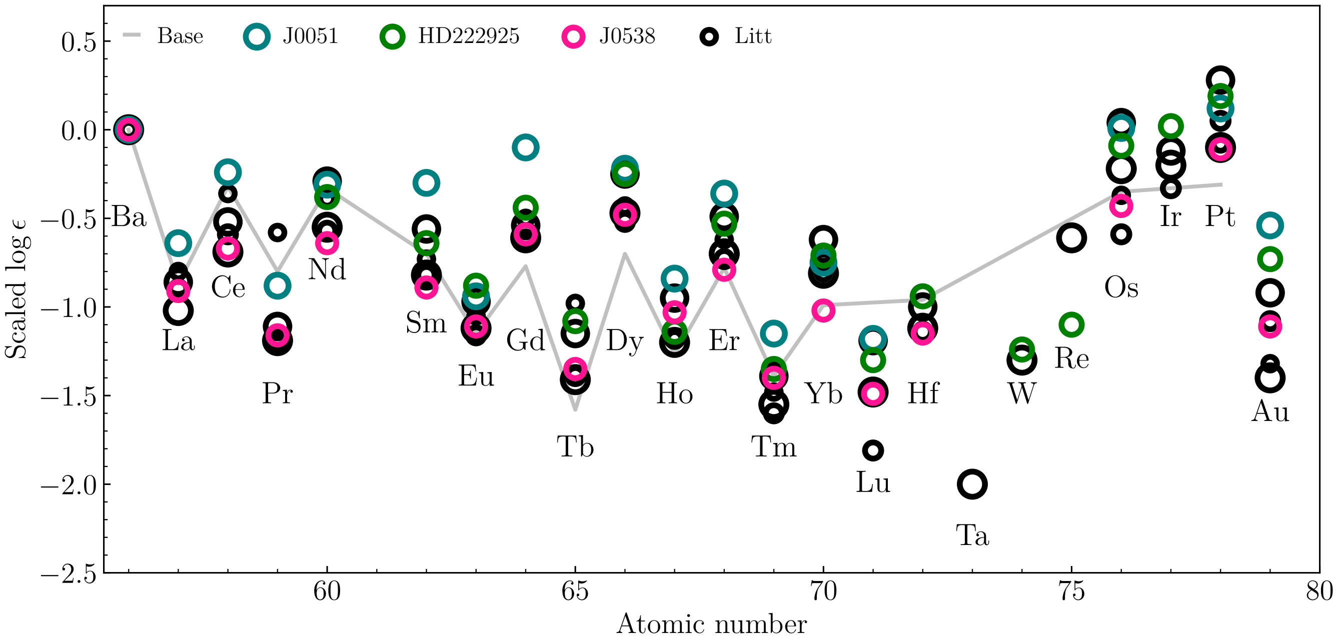

Fig. 5. Absolute abundances of heavy *r*-process elements in the three RPA HST stars (pink, green, and blue) and literature stars (black) with Au detections compared to the baseline pattern from Roederer et al. (2023). Point size is correlated with the Eu abundance of the star. A somewhat larger star-to-star scatter is seen for Au compared to the other elements. (Note that Roederer et al. (2023) did not include Lu, Ta, W, Re, and Ir in their sample; hence, the baseline pattern (grey line) in Figure 5 is not representative for these two elements.)

scatter is detected, and no clear correlation with Eu abundances is seen as is found for other elements affected by fission fragment deposition. However, Shah et al. (2024) found correlations between the derived Cd abundances stellar parameters, suggesting current Cd abundances are affected by non-LTE effects, which may also be the case for the Au abundances similarly derived from neutral species.

Acknowledgements. We acknowledge generous support provided by NASA through grant GO-15951 from the Space Telescope Science Institute, which is operated by the Association of Universities for Research in Astronomy, Incorporated, under NASA contract NAS5-26555. TTH acknowledges support from the Swedish Research Council (VR 2021-05556). EMH acknowledges this work performed under the auspices of the U.S. Department of Energy by Lawrence Livermore National Laboratory under Contract DE-AC52-07NA27344. This research has made use of NASA's Astrophysics Data System Bibliographic Services; the arXiv.org preprint server operated by Cornell University; the SIMBAD and VizieR databases hosted by the Strasbourg Astronomical Data Center (Wenger et al. 2000); the ASD hosted by NIST; the MAST at STScI; Image Reduction and Analysis Facility (IRAF) NOIRLab IRAF is distributed by the Community Science and Data Center at NSF NOIRLab, which is managed by the Association of Universities for Research in Astronomy (AURA) under a cooperative agreement with the U.S. National Science Foundation (Tody 1986, 1993; Fitzpatrick et al. 2024); NumPy (van der Walt et al. 2011); Matplotlib (Hunter 2007); and AstroPy (Astropy Collaboration et al. 2013, 2018)

References

Abbott, B. P., Abbott, R., Abbott, T. D., et al. 2017, Physical Review Letters, 119, 161101
Aoki, W., Beers, T. C., Christlieb, N., et al. 2007, ApJ, 655, 492
Asplund, M., Grevesse, N., Sauval, A. J., & Scott, P. 2009, ARA&A, 47, 481
Astropy Collaboration, Price-Whelan, A. M., Sipőcz, B. M., et al. 2018, AJ, 156, 123
Astropy Collaboration, Robitaille, T. P., Tollerud, E. J., et al. 2013, A&A, 558, A33
Babusiaux, C., Fabricius, C., Khanna, S., et al. 2023, A&A, 674, A32
Bailer-Jones, C. A. L., Rybizki, J., Fouesneau, M., Demleitner, M., & Andrae, R. 2021, AJ, 161, 147
Bandyopadhyay, A., Ezzeddine, R., Allende Prieto, C., et al. 2024, ApJS, 274, 39
Beers, T. C. & Christlieb, N. 2005, ARA&A, 43, 531
Belmonte, M. T., Pickering, J. C., Ruffoni, M. P., et al. 2017, ApJ, 848, 125
Bergemann, M. & Cescutti, G. 2010, A&A, 522, A9
Bergemann, M. & Gehren, T. 2008, A&A, 492, 823
Bergemann, M., Kudritzki, R.-P., Würl, M., et al. 2013, ApJ, 764, 115
Bergemann, M., Pickering, J. C., & Gehren, T. 2010, MNRAS, 401, 1334
Bernstein, R., Shectman, S. A., Gunnels, S. M., Mochnacki, S., & Athey, A. E. 2003, in Society of Photo-Optical Instrumentation Engineers (SPIE) Conference Series, Vol. 4841, Instrument Design and Performance for Optical/Infrared Ground-based Telescopes, ed. M. Iye & A. F. M. Moorwood, 1694–1704
Biémont, É., Blagoev, K., Engström, L., et al. 2011, MNRAS, 414, 3350
Bowen, I. S. & Vaughan, A. H., J. 1973, Appl. Opt., 12, 1430
Burbidge, E. M., Burbidge, G. R., Fowler, W. A., & Hoyle, F. 1957, Reviews of Modern Physics, 29, 547
Cain, M., Frebel, A., Ji, A. P., et al. 2020, ApJ, 898, 40
Cameron, A. G. W. 1957, PASP, 69, 201
Casagrande, L. & VandenBerg, D. A. 2014, MNRAS, 444, 392
Castelli, F. & Kurucz, R. L. 2003, in Modelling of Stellar Atmospheres, ed. N. Piskunov, W. W. Weiss, & D. F. Gray, Vol. 210, A20
Côté, B., Belczynski, K., Fryer, C. L., et al. 2017, ApJ, 836, 230
Côté, B., Fryer, C. L., Belczynski, K., et al. 2018, ApJ, 855, 99
Cowan, J. J., Sneden, C., Burles, S., et al. 2002, ApJ, 572, 861
Cutri, R. M., Skrutskie, M. F., van Dyk, S., et al. 2003, VizieR Online Data Catalog, II/246
Demidov, Y. A., Konovalova, E. A., Imanbaeva, R. T., Kozlov, M. G., & Barzakh, A. E. 2021, Phys. Rev. A, 103, 032824
Den Hartog, E. A., Herd, M. T., Lawler, J. E., et al. 2005, ApJ, 619, 639
Den Hartog, E. A., Lawler, J. E., & Roederer, I. U. 2020, ApJS, 248, 10
Den Hartog, E. A., Lawler, J. E., & Roederer, I. U. 2021a, ApJS, 254, 5
Den Hartog, E. A., Lawler, J. E., Sneden, C., & Cowan, J. J. 2003, ApJS, 148, 543
Den Hartog, E. A., Lawler, J. E., Sneden, C., & Cowan, J. J. 2006, ApJS, 167, 292
Den Hartog, E. A., Lawler, J. E., Sneden, C., Cowan, J. J., & Brukhovesky, A. 2019, ApJS, 243, 33
Den Hartog, E. A., Lawler, J. E., Sneden, C., et al. 2021b, ApJS, 255, 27
Den Hartog, E. A., Lawler, J. E., Sneden, C., Roederer, I. U., & Cowan, J. J. 2023, ApJS, 265, 42

Den Hartog, E. A., Lawler, J. E., Sobeck, J. S., Sneden, C., & Cowan, J. J. 2011, ApJS, 194, 35

Den Hartog, E. A., Ruffoni, M. P., Lawler, J. E., et al. 2014, ApJS, 215, 23

Drout, M. R., Piro, A. L., Shappee, B. J., et al. 2017, Science, 358, 1570

Eichler, M., Arcones, A., Kelic, A., et al. 2015, ApJ, 808, 30

Eitner, P., Bergemann, M., Ruiter, A. J., et al. 2023, A&A, 677, A151

Ezzeddine, R., Rasmussen, K., Frebel, A., et al. 2020, ApJ, 898, 150

Fedchak, J. A. & Lawler, J. E. 1999, ApJ, 523, 734

Fitzpatrick, M., Placco, V., Bolton, A., et al. 2024, arXiv e-prints, arXiv:2401.01982

Fivet, V., Quinet, P., Biémont, É., & Xu, H. L. 2006, Journal of Physics B Atomic Molecular Physics, 39, 3587

Fujimoto, S.-i., Nishimura, N., & Hashimoto, M.-a. 2008, ApJ, 680, 1350

Fulbright, J. P. 2000, AJ, 120, 1841

Gaia Collaboration. 2018, VizieR Online Data Catalog, I/345

Gaia Collaboration, Vallenari, A., Brown, A. G. A., et al. 2023, A&A, 674, A1

Grichener, A. & Soker, N. 2019, ApJ, 878, 24

Gudin, D., Shank, D., Beers, T. C., et al. 2021, ApJ, 908, 79

Gurell, J., Nilsson, H., Engström, L., et al. 2010, A&A, 511, A68

Hannaford, P., Larkins, P. L., & Lowe, R. M. 1981, Journal of Physics B Atomic Molecular Physics, 14, 2321

Hansen, T. T., Beers, T. C., Ezzeddine, R., et al. 2019, Testing r-process nucleosynthesis models with two r-process enhanced stars, HST Proposal. Cycle 27, ID. #15951

Hansen, T. T., Holmbeck, E. M., Beers, T. C., et al. 2018, ApJ, 858, 92

Holmbeck, E. M., Beers, T. C., Roederer, I. U., et al. 2018, ApJ, 859, L24

Holmbeck, E. M., Hansen, T. T., Beers, T. C., et al. 2020, ApJS, 249, 30

Hunter, J. D. 2007, Computing in Science and Engineering, 9, 90

Ivans, I. I., Simmerer, J., Sneden, C., et al. 2006, ApJ, 645, 613

Ji, A. P., Li, T. S., Hansen, T. T., et al. 2020, AJ, 160, 181

Kelson, D. D. 2003, PASP, 115, 688

Kimble, R. A., Woodgate, B. E., Bowers, C. W., et al. 1998, ApJ, 492, L83

Kramida, A., Ralchenko, Y., Nave, G., & Reader, J. 2018, in APS Meeting Abstracts, Vol. 2018, APS Division of Atomic, Molecular and Optical Physics Meeting Abstracts, M01.004

Kramida, A., Ralchenko, Y., Reader, J., & NIST ASD Team. 2020, National Institute of Standards and Technology, Gaithersburg, MD.

Kurucz, R. L. 2011, Canadian Journal of Physics, 89, 417

Lattimer, J. M. & Schramm, D. N. 1974, ApJ, 192, L145

Lawler, J. E., Bonvallet, G., & Sneden, C. 2001a, ApJ, 556, 452

Lawler, J. E. & Dakin, J. T. 1989, Journal of the Optical Society of America B Optical Physics, 6, 1457

Lawler, J. E., den Hartog, E. A., Labby, Z. E., et al. 2007, ApJS, 169, 120

Lawler, J. E., Den Hartog, E. A., Sneden, C., & Cowan, J. J. 2006, ApJS, 162, 227

Lawler, J. E., Feigenson, T., Sneden, C., Cowan, J. J., & Nave, G. 2018, ApJS, 238, 7

Lawler, J. E., Guzman, A., Wood, M. P., Sneden, C., & Cowan, J. J. 2013, ApJS, 205, 11

Lawler, J. E., Hala, Sneden, C., et al. 2019, ApJS, 241, 21

Lawler, J. E., Sneden, C., & Cowan, J. J. 2004, ApJ, 604, 850

Lawler, J. E., Sneden, C., & Cowan, J. J. 2015, ApJS, 220, 13

Lawler, J. E., Sneden, C., Cowan, J. J., Ivans, I. I., & Den Hartog, E. A. 2009, ApJS, 182, 51

Lawler, J. E., Sneden, C., Cowan, J. J., et al. 2008, ApJS, 178, 71

Lawler, J. E., Sneden, C., Nave, G., et al. 2017, ApJS, 228, 10

Lawler, J. E., Wickliffe, M. E., Cowley, C. R., & Sneden, C. 2001b, ApJS, 137, 341

Lawler, J. E., Wickliffe, M. E., den Hartog, E. A., & Sneden, C. 2001c, ApJ, 563, 1075

Lawler, J. E., Wyart, J. F., & Blaise, J. 2001d, ApJS, 137, 351

Li, R., Chatelain, R., Holt, R. A., et al. 2007, Phys. Scr, 76, 577

Lind, K., Nordlander, T., Wehrhahn, A., et al. 2022, A&A, 665, A33

Ljung, G., Nilsson, H., Asplund, M., & Johansson, S. 2006, A&A, 456, 1181

Lund, K. A., Engel, J., McLaughlin, G. C., et al. 2023, ApJ, 944, 144

Maeder, A. & Meynet, G. 2015, A&A, 580, A32

Malcheva, G., Blagoev, K., Mayo, R., et al. 2006, MNRAS, 367, 754

Mallinson, J. W. E., Lind, K., Amarsi, A. M., et al. 2022, A&A, 668, A103

McCall, M. L. 2004, AJ, 128, 2144

McWilliam, A. 1998, AJ, 115, 1640

Meléndez, J. & Barbuy, B. 2009, A&A, 497, 611

Mucciarelli, A., Bellazzini, M., & Massari, D. 2021, A&A, 653, A90

Munari, U., Henden, A., Frigo, A., et al. 2014, AJ, 148, 81

Nilsson, H., Hartman, H., Engström, L., et al. 2010, A&A, 511, A16

Nilsson, H., Ljung, G., Lundberg, H., & Nielsen, K. E. 2006, A&A, 445, 1165

Nilsson, H., Zhang, Z. G., Lundberg, H., Johansson, S., & Nordström, B. 2002, A&A, 382, 368

O'Brian, T. R., Wickliffe, M. E., Lawler, J. E., Whaling, W., & Brault, J. W. 1991, Journal of the Optical Society of America B Optical Physics, 8, 1185

Pakhomov, Y. V., Ryabchikova, T. A., & Piskunov, N. E. 2019, Astronomy Reports, 63, 1010

Pehlivan Rhodin, A., Hartman, H., Nilsson, H., & Jönsson, P. 2017, A&A, 598, A102

Peterson, R. C., Barbuy, B., & Spite, M. 2020, A&A, 638, A64

Pickering, J. C., Thorne, A. P., & Perez, R. 2001, ApJS, 132, 403

Pickering, J. C., Thorne, A. P., & Perez, R. 2002, ApJS, 138, 247

Piskunov, N. E., Kupka, F., Ryabchikova, T. A., Weiss, W. W., & Jeffery, C. S. 1995, A&AS, 112, 525

Placco, V. M., Santucci, R. M., Yuan, Z., et al. 2020, ApJ, 897, 78

Placco, V. M., Sneden, C., Roederer, I. U., et al. 2021, Research Notes of the American Astronomical Society, 5, 92

Roederer, I. U., Cowan, J. J., Pignatari, M., et al. 2022a, ApJ, 936, 84

Roederer, I. U., Hattori, K., & Valluri, M. 2018a, AJ, 156, 179

Roederer, I. U. & Lawler, J. E. 2012, ApJ, 750, 76

Roederer, I. U. & Lawler, J. E. 2021, ApJ, 912, 119

Roederer, I. U., Lawler, J. E., Den Hartog, E. A., et al. 2022b, ApJS, 260, 27

Roederer, I. U., Lawler, J. E., Sneden, C., et al. 2008, ApJ, 675, 723

Roederer, I. U., Lawler, J. E., Sobeck, J. S., et al. 2012, ApJS, 203, 27

Roederer, I. U., Preston, G. W., Thompson, I. B., et al. 2014a, AJ, 147, 136

Roederer, I. U., Sakari, C. M., Placco, V. M., et al. 2018b, ApJ, 865, 129

Roederer, I. U., Schatz, H., Lawler, J. E., et al. 2014b, ApJ, 791, 32

Roederer, I. U., Sneden, C., Lawler, J. E., & Cowan, J. J. 2010, ApJ, 714, L123

Roederer, I. U., Vassh, N., Holmbeck, E. M., et al. 2023, Science, 382, 1177

Ruffoni, M. P., Den Hartog, E. A., Lawler, J. E., et al. 2014, MNRAS, 441, 3127

Sakari, C. M., Placco, V. M., Hansen, T., et al. 2018, ApJ, 854, L20

Schlafly, E. F. & Finkbeiner, D. P. 2011, ApJ, 737, 103

Shah, S. P., Ezzeddine, R., Roederer, I. U., et al. 2024, MNRAS, 529, 1917

Shank, D., Beers, T. C., Placco, V. M., et al. 2023, ApJ, 943, 23

Siegel, D. M., Barnes, J., & Metzger, B. D. 2019, Nature, 569, 241

Sikström, C. M., Pihlemark, H., Nilsson, H., et al. 2001, Journal of Physics B Atomic Molecular Physics, 34, 477

Siqueira Mello, C., Spite, M., Barbuy, B., et al. 2013, A&A, 550, A122

Sneden, C., Cowan, J. J., & Gallino, R. 2008, ARA&A, 46, 241

Sneden, C., Cowan, J. J., Lawler, J. E., et al. 2003, ApJ, 591, 936

Sneden, C., Lawler, J. E., Cowan, J. J., Ivans, I. I., & Den Hartog, E. A. 2009, ApJS, 182, 80

Sneden, C. A. 1973, PhD thesis, University of Texas, Austin

Sobeck, J. S., Kraft, R. P., Sneden, C., et al. 2011, AJ, 141, 175

Sobeck, J. S., Lawler, J. E., & Sneden, C. 2007, ApJ, 667, 1267

Surman, R. & Engel, J. 2001, Phys. Rev. C, 64, 035801

Tody, D. 1986, in Society of Photo-Optical Instrumentation Engineers (SPIE) Conference Series, Vol. 627, Instrumentation in astronomy VI, ed. D. L. Crawford, 733

Tody, D. 1993, in Astronomical Society of the Pacific Conference Series, Vol. 52, Astronomical Data Analysis Software and Systems II, ed. R. J. Hanisch, R. J. V. Brissenden, & J. Barnes, 173

Träbert, E., Wolf, A., Linkemann, J., & Tordoir, X. 1999, Journal of Physics B Atomic Molecular Physics, 32, 537

van der Walt, S., Colbert, S. C., & Varoquaux, G. 2011, Computing in Science and Engineering, 13, 22

Wehmeyer, B., Fröhlich, C., Côté, B., Pignatari, M., & Thielemann, F. K. 2019, MNRAS, 487, 1745

Wenger, M., Ochsenbein, F., Egret, D., et al. 2000, A&AS, 143, 9

Wickliffe, M. E. & Lawler, J. E. 1997, Journal of the Optical Society of America B Optical Physics, 14, 737

Wickliffe, M. E., Lawler, J. E., & Nave, G. 2000, J. Quant. Spectr. Rad. Transf., 66, 363

Wood, M. P., Lawler, J. E., Den Hartog, E. A., Sneden, C., & Cowan, J. J. 2014a, ApJS, 214, 18

Wood, M. P., Lawler, J. E., Sneden, C., & Cowan, J. J. 2013, ApJS, 208, 27

Wood, M. P., Lawler, J. E., Sneden, C., & Cowan, J. J. 2014b, ApJS, 211, 20

Woodgate, B. E., Kimble, R. A., Bowers, C. W., et al. 1998, PASP, 110, 1183

Xu, H. L., Persson, A., Svanberg, S., et al. 2004, Phys. Rev. A, 70, 042508

Yoon, J., Beers, T. C., Placco, V. M., et al. 2016, ApJ, 833, 20

Table 4. Abundance Summary for J0538.

El.	N	log ϵ (X)	[X/H]	$\sigma_{[X/H]}$ [dex]	[X/Fe]	$\sigma_{[X/Fe]}$ [dex]
CH	1	< +4.88	< −3.55	...	< −0.96	...
NH	1	< +5.93	< −1.90	...	< +0.70	...
O I	3	+7.13	−1.56	0.06	+1.03	0.07
Na I	2	+4.54	−1.70	0.20	+0.90	0.20
Mg I	12	+5.47	−2.13	0.04	+0.46	0.04
Al I	5	+3.28	−3.17	0.18	−0.57	0.17
Al II	1	+3.87	−2.58	0.23	+0.02	0.23
Si I	4	+5.22	−2.29	0.10	+0.30	0.10
Si II	2	+5.67	−1.84	0.19	+0.75	0.20
P I	1	+2.69	−2.72	0.26	−0.13	0.26
K I	2	+3.28	−1.75	0.17	+0.84	0.17
Ca I	19	+4.14	−2.20	0.04	+0.40	0.04
Sc II	12	+0.83	−2.32	0.06	+0.27	0.07
Ti I	16	+2.80	−2.15	0.05	+0.44	0.05
Ti II	36	+2.82	−2.13	0.04	+0.47	0.05
V II	23	+1.59	−2.34	0.04	+0.25	0.05
Cr I	11	+2.93	−2.71	0.05	−0.12	0.05
Cr II	15	+3.24	−2.40	0.04	+0.19	0.05
Mn I	7	+2.32	−3.11	0.08	−0.52	0.08
Mn II	5	+2.56	−2.87	0.07	−0.28	0.08
Fe I	115	+4.91	−2.59	0.02	...	...
Fe II	13	+4.98	−2.52	0.04	+0.08	...
Co I	18	+2.49	−2.50	0.06	+0.09	0.06
Co II	6	+2.48	−2.51	0.11	+0.08	0.11
Ni I	28	+3.65	−2.57	0.04	+0.02	0.04
Ni II	4	+3.90	−2.32	0.29	+0.27	0.29
Cu I	1	< +0.91	< −3.28	...	< −0.69	...
Zn II	3	+2.33	−2.23	0.04	+0.36	0.04
Sr II	2	+1.46	−1.41	0.22	+1.18	0.21
Y II	16	−0.02	−2.23	0.04	+0.36	0.05
Zr II	26	+0.68	−1.90	0.04	+0.69	0.05
Nb II	3	−0.34	−1.80	0.16	+0.79	0.16
Mo II	4	+0.14	−1.74	0.08	+0.86	0.08
Cd I	1	−0.36	−2.07	0.26	+0.52	0.26
Ba II	4	+0.33	−1.85	0.13	+0.74	0.13
La II	14	−0.58	−1.68	0.06	+0.91	0.06
Ce II	12	−0.34	−1.92	0.02	+0.68	0.05
Pr II	3	−0.83	−1.55	0.13	+1.05	0.13
Nd II	19	−0.31	−1.73	0.04	+0.87	0.06
Sm II	21	−0.56	−1.52	0.05	+1.08	0.06
Eu II	7	−0.78	−1.30	0.08	+1.29	0.08
Gd II	11	−0.26	−1.33	0.04	+1.26	0.05
Tb II	2	−1.02	−1.32	0.20	+1.27	0.20
Dy II	13	−0.15	−1.25	0.04	+1.34	0.05
Ho II	4	−0.70	−1.18	0.09	+1.42	0.09
Er II	5	−0.46	−1.38	0.08	+1.21	0.08
Tm II	2	−1.07	−1.17	0.18	+1.42	0.18
Yb II	1	−0.69	−1.53	0.27	+1.06	0.26
Lu II	1	−1.16	−1.26	0.25	+1.33	0.26
Hf II	2	−0.82	−1.67	0.24	+0.93	0.24
Os II	1	−0.10	−1.50	0.27	+1.09	0.27
Pt I	4	+0.22	−1.40	0.17	+1.20	0.17
Au I	2	−0.78	−1.70	0.21	+0.89	0.21
Th II	1	−1.16	−1.18	0.23	+1.41	0.23

Table 5. Abundance uncertainties for J0538.

El	$\Delta_{T_{\rm eff}}$ [dex]	$\Delta_{\log g}$ [dex]	Δ_{ξ} [dex]	$\Delta_{[M/H]}$ [dex]	s_X [dex]
O I	-0.052	0.031	-0.003	-0.011	0.100
Na I	0.037	0.003	-0.067	-0.016	0.238
Mg I	0.032	-0.011	-0.022	0.001	0.139
Al I	0.071	-0.000	-0.015	0.010	0.347
Al II	0.025	0.019	0.014	0.011	0.224
Si I	0.057	-0.012	-0.044	-0.007	0.156
Si II	-0.022	-0.030	-0.061	-0.049	0.224
P I	0.117	-0.008	-0.008	0.014	0.224
K I	0.038	-0.002	-0.004	0.004	0.234
Ca I	0.036	-0.002	-0.004	0.005	0.125
Sc II	0.013	0.018	-0.009	0.002	0.168
Ti I	0.059	-0.005	0.001	0.009	0.124
Ti II	0.021	0.021	-0.012	0.000	0.142
V II	0.013	0.016	0.001	0.003	0.161
Cr I	0.053	-0.007	-0.006	0.007	0.143
Cr II	0.005	0.010	-0.006	0.000	0.156
Mn I	0.046	-0.011	0.001	0.011	0.175
Mn II	0.011	0.010	-0.008	0.005	0.142
Fe I	0.049	-0.004	-0.005	0.005	0.123
Fe II	0.015	0.022	-0.013	0.002	0.143
Co I	0.068	-0.012	0.004	0.010	0.166
Co II	0.030	0.043	-0.001	0.019	0.201
Ni I	0.049	-0.009	-0.030	0.000	0.139
Ni II	-0.001	0.017	-0.047	-0.017	0.566
Zn II	0.041	0.000	-0.001	0.006	0.100
Sr II	0.047	0.021	-0.088	-0.011	0.225
Y II	0.022	0.017	-0.002	0.005	0.121
Zr II	0.026	0.017	0.002	0.009	0.150
Nb II	0.048	0.034	0.002	0.017	0.141
Mo II	0.056	0.011	0.002	0.014	0.100
Cd I	0.062	-0.006	0.014	0.013	0.224
Ba II	0.038	0.023	-0.035	-0.005	0.185
La II	0.023	0.023	0.007	0.011	0.144
Ce II	0.013	0.018	0.021	0.013	0.100
Pr II	0.023	0.029	0.028	0.025	0.141
Nd II	0.015	0.012	0.013	0.012	0.157
Sm II	0.013	0.017	0.010	0.012	0.141
Eu II	0.030	0.020	0.007	0.011	0.143
Gd II	0.003	0.018	0.021	0.010	0.115
Tb II	0.013	0.024	0.029	0.010	0.245
Dy II	0.021	0.020	0.001	0.008	0.134
Ho II	0.035	0.013	0.004	0.009	0.147
Er II	0.036	0.014	0.005	0.014	0.153
Tm II	0.000	0.017	0.024	0.003	0.224
Yb II	0.078	0.021	-0.016	0.010	0.245
Lu II	-0.003	0.004	-0.003	0.003	0.245
Hf II	0.002	0.008	0.007	0.008	0.224
Os II	0.011	0.016	0.015	0.004	0.224
Pt I	0.061	-0.013	0.006	0.010	0.310
Au I	0.099	-0.002	0.006	0.015	0.245
Th II	0.008	0.012	-0.000	0.002	0.224

Appendix A: Atomic data

Table A.1. Atomic data and abundances for individual lines analysed.

λ (Å)	species	χ (eV)	$\log gf$	EW (mÅ)	$\log \epsilon(X)$ (dex)	Ref
7771.94	8.0	9.15	+0.37	26.64	+7.13	1
7774.17	8.0	9.15	+0.22	21.02	+7.14	1
7775.39	8.0	9.15	0.00	13.73	+7.12	1
5889.95	11.0	0.00	+0.11	177.37	+4.62	1
5895.92	11.0	0.00	−0.19	150.18	+4.46	1
2776.69	12.0	2.71	−0.12	syn	+5.39	1
2779.83	12.0	2.72	+0.38	syn	+5.37	1
2782.97	12.0	2.72	−0.12	syn	+5.43	1
2846.72	12.0	2.71	−1.32	syn	+5.31	1
3829.35	12.0	2.71	−0.23	166.60	+5.60	1
3986.75	12.0	4.35	−1.06	22.42	+5.55	1
4057.51	12.0	4.35	−0.90	23.82	+5.42	1

References. (1) NIST Kramida et al. (2020); (2) Pehlivan Rhodin et al. (2017); (3) = NIST Kramida et al. (2020) for log(gf) value and VALD Piskunov et al. (1995); Pakhomov et al. (2019) for HFS; (4) Träbert et al. (1999) for log(gf) value and Roederer & Lawler (2021) for HFS; (5) Den Hartog et al. (2023); (6) Den Hartog et al. (2021b); (7) Lawler & Dakin (1989) for logg and Kurucz (2011) for HFS; (8) Lawler et al. (2019); (9) Lawler et al. (2013); (10) Wood et al. (2013); (11) Pickering et al. (2001), with corrections given in Pickering et al. (2002); (12) Wood et al. (2014a) for log(gf) value and HFS; (13) Sobeck et al. (2007), (14) Lawler et al. (2017), (15) Gurell et al. (2010); (16) Nilsson et al. (2006); (17) Den Hartog et al. (2011) for both log(gf) value and hfs; (18) O'Brian et al. (1991); (19) Belmonte et al. (2017); (20) Den Hartog et al. (2014); (21) Ruffoni et al. (2014); (22) Den Hartog et al. (2019); (23) Meléndez & Barbuy (2009); (24) Lawler et al. (2015) for log(gf) values and HFS; (25) Lawler et al. (2018) for log(gf) value and Roederer et al. (2022b)for HFS; (26) Wood et al. (2014b); (27) Fedchak & Lawler (1999); (28) Roederer & Lawler (2012); (29) Biémont et al. (2011); (30) Ljung et al. (2006); (31) Malcheva et al. (2006); (32) Nilsson et al. (2010), including HFS; (33) Sikström et al. (2001); (34) Xu et al. (2004); (35) Kramida et al. (2018), using HFS/IS from McWilliam (1998); (36) Lawler et al. (2001a), using HFS from Ivans et al. (2006) when available; (37) Lawler et al. (2009); (38) Li et al. (2007), using HFS from Sneden et al. (2009); (39) Den Hartog et al. (2003), using HFS/IS from Roederer et al. (2008) when available; (40) Lawler et al. (2006), using HFS/IS from Roederer et al. (2008) when available; (41) Lawler et al. (2001c), using HFS/IS from Ivans et al. (2006); (42) Den Hartog et al. (2006), (43) Lawler et al. (2001b), using HFS from Lawler et al. (2001d); (44) Wickliffe et al. (2000); (45) Lawler et al. (2004), using HFS from Lawler et al. (2009); (46) Lawler et al. (2008); (47) Wickliffe & Lawler (1997); (48) Sneden et al. (2009) for log(gf) value and HFS/IS; (49) Roederer et al. (2010) for log(gf) value and Den Hartog et al. (2020) for HFS; (50) Den Hartog et al. (2021a); (51) Lawler et al. (2007); (52) Den Hartog et al. (2005) for log(gf) value and HFS/IS; (54) Den Hartog et al. (2005) for log(gf) value only; (55) Hannaford et al. (1981) for log(gf) value and Demidov et al. (2021)for HFS; (56) Nilsson et al. (2002)

Notes. The complete version of this table is available online only. A subset is shown here to illustrate its form and content.